A mitochondria-regulated p53-CCF circuit integrates genome integrity with inflammation

Karl N. Miller[1]*, Brightany Li[1], Hannah R. Pierce-Hoffman[1], Xue Lei[1], Aaron P. Havas[1], Shreeya Patel[1], Carolina Cano Macip[1], Stella G. Victorelli[2,3], Seung-Hwa Woo[2,3], Anthony B. Lagnado[2,3], Tianhui Liu[1], Nirmalya Dasgupta[1,4], Jun Lyu[5], Yoav Altman[6], Rebecca A. Porritt[6], Guillermina Garcia[6], Carolin Mogler[7], Zhixun Dou[8,9], Chongyi Chen[5], João F. Passos[2,3], and Peter D. Adams[1]*

[1]Cancer Genome and Epigenetics Program; Sanford Burnham Prebys MDI; La Jolla, CA, USA
[2]Department of Physiology and Biomedical Engineering; Mayo Clinic; Rochester, MN, USA
[3]Robert and Arlene Kogod Center on Aging; Mayo Clinic; Rochester, MN, USA
[4]Center for Cancer Therapy; La Jolla Institute of Immunology; La Jolla, CA
[5]Laboratory of Biochemistry and Molecular Biology; National Cancer Institute; National Institutes of Health; Bethesda, MD, USA
[6]Shared Resources; NCI-designated Cancer Center; Sanford Burnham Prebys MDI; La Jolla, CA, USA
[7]Institute of Pathology; School of Medicine and Health; Technical University Munich (TUM); Munich, Germany
[8]Center for Regenerative Medicine, Department of Medicine; Massachusetts General Research Institute; Boston, MA, USA
[9]Harvard Stem Cell Institute; Harvard University; Cambridge, MA, USA
*Correspondence: kmiller@sbpdiscovery.org, padams@sbpdiscovery.org

Karl N. Miller	kmiller@sbpdiscovery.org
Brightany Li	bli@sbpdiscovery.org
Hannah R. Pierce-Hoffman	hrp2112@columbia.edu
Xue Lei	xlei@sbpdiscovery.org
Aaron P. Havas	ahavas@sbpdiscovery.org
Shreeya Patel	spatel@sbpdiscovery.org
Carolina Cano Macip	ccanomacip@sbpdiscovery.org
Stella G. Victorelli	victorelli.stella@mayo.edu
Seung-Hwa Woo	woo.seunghwa@mayo.edu
Anthony B. Lagnado	lagnado.anthony@mayo.edu
Tianhui Liu	tianhuil@sbpdiscovery.org
Nirmalya Dasgupta	ndasgupta@lji.org
Jun Lyu	jun.lyu@nih.gov
Yoav Altman	yoav@sbpdiscovery.org
Rebecca A. Porritt	rporritt@sbpdiscovery.org
Guillermina Garcia	ggarcia@sbpdiscovery.org
Carolin Mogler	carolin.mogler@tum.de
Zhixun Dou	zdou@mgh.harvard.edu
Chongyi Chen	chongyi.chen@nih.gov
João F. Passos	passos.joao@mayo.edu
Peter D. Adams	padams@sbpdiscovery.org

Abstract

Genomic instability and inflammation are distinct hallmarks of aging, but the connection between them is poorly understood. Understanding their interrelationship will help unravel new mechanisms and therapeutic targets of aging and age-associated diseases. Here we report a novel mechanism directly linking genomic instability and inflammation in senescent cells, through a mitochondria-regulated molecular circuit that connects the p53 tumor suppressor and cytoplasmic chromatin fragments (CCF), a driver of inflammation through the cGAS-STING pathway. Activation or inactivation of p53 by genetic and pharmacologic approaches showed that p53 suppresses CCF accumulation and the downstream inflammatory senescence-associated secretory phenotype (SASP), independent of its effects on cell cycle arrest. p53 activation suppressed CCF formation by promoting DNA repair, reflected in maintenance of genomic integrity, particularly in subtelomeric regions, as shown by single cell genome resequencing. Activation of p53 by pharmacological inhibition of MDM2 in old mice decreased features of SASP in liver, indicating a senomorphic role *in vivo*. Remarkably, mitochondria in senescent cells suppressed p53 activity by promoting CCF formation and thereby restricting ATM-dependent nuclear DNA damage signaling. These data provide evidence for a mitochondria-regulated p53-CCF circuit in senescent cells that controls DNA repair, genome integrity and inflammatory SASP, and is a potential target for senomorphic healthy aging interventions.

Introduction

Cellular senescence is a cell fate initiated by severe cellular stress and characterized by specific phenotypes, including stable cell cycle exit[1] and development of a heterogeneous, pro-inflammatory senescence-associated secretory phenotype (SASP)[2]. The SASP contributes to chronic disease vulnerability and frailty in aged animals[3,4], which has led to efforts in development of therapies targeting senescent cells or senescence phenotypes to promote healthy aging[5-8]. “Senolytic” approaches that target and remove senescent cells are one area of intensive investigation, but they are still in early stages of potential clinical translation[9].

An alternative approach to modulate senescence function, a so-called “senomorphic” approach, targets the SASP specifically. Although senomorphic approaches show some promise for reducing chronic disease burden such as cancer *in vivo*[10-16], the molecular regulation of SASP and relevance to age-associated disease vulnerability are poorly understood. There are many known regulators of the SASP, including mTOR[10], GATA4[17], p38MAPK[18] and p53[2]. Paradoxically, p53, a master inducer of senescence, has been reported to be a suppressor of SASP[2]. A molecular explanation of this paradox has been lacking.

The SASP is also induced by cytoplasmic DNA[19] such as LINE1[20] and mtDNA[21]. We have previously shown that the SASP is driven by a mitochondria-nucleus retrograde signaling pathway that promotes expulsion of cytoplasmic chromatin fragments (CCF) from the nucleus to the cytoplasm of senescent cells[22]. CCF are sensed by the cGAS/STING pathway, which activates the master transcriptional regulator of the SASP, NFkB[23-26]. However, the molecular regulation of CCF formation and the possibility of targeting this pathway in aged tissue *in vivo* remain unclear. Here, we identify a p53-regulated pathway that is subject to mitochondrial control, which suppresses CCF formation and the SASP, while also promoting DNA repair and genome integrity of senescent cells. We show that this pathway is pharmacologically targetable in cultured cells and mice, validating it as a target for senomorphic interventions and highlighting a novel function of p53 in safeguarding genome integrity of senescent cells.

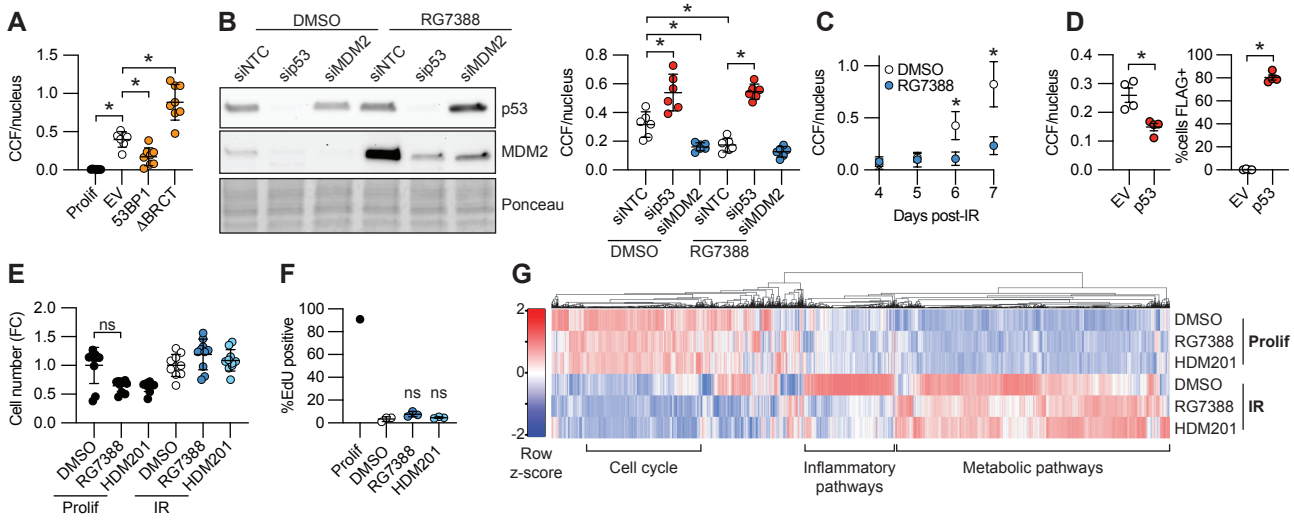

Figure 1: p53 suppresses CCF formation. A) CCF staining by IF in irradiation-induced senescent IMR90 human fibroblasts. Each value represents an individual well from a culture plate, from a representative experiment. B) Western blot and CCF staining by immunofluorescence using timeframe described in Fig.S1J, representative of n=2 experiments. C) CCF staining by IF, average of 3 experiments. D) CCF and FLAG staining by IF. Each value represents a separate infection in a single experiment, representative of n=3 experiments. E) Cell number normalized to DMSO control for each group. F) EdU incorporation assay. G) Differentially expressed genes by RNAseq, n=3 per group with summarized KEGG ontology for each major cluster. See Table S1 for detailed ontology. Data shown as means ±SEM, asterisk(*) indicates $p<0.05$ by Student's t-test. Prolif: proliferating control; EV: empty vector; NTC: non-targeting contro; IR: ionizing radiation-induced senescence.

p53 suppresses CCF formation

The molecular regulation of CCF formation is poorly understood[27]. We have previously shown that the DNA repair protein 53BP1 is a suppressor of CCF formation and the SASP[22]. To determine the molecular role of 53BP1 in CCF formation, we developed a 53BP1 exogenous expression-based CCF suppression assay with modest overexpression of 53BP1 in irradiation-induced senescent IMR90 primary human fibroblasts. Western blot, qPCR, and RNA-seq confirmed specific suppression of SASP by modest 53BP1 overexpression (Fig.S1A-E, Table S1), with no effect on the upregulation of cell cycle inhibitors and downregulation of cell cycle genes. We next mutated known functional domains of 53BP1 and tested their ability to suppress CCF formation (Fig.S1F-G). Analysis of these 53BP1 mutants showed that the tandem BRCT domains of 53BP1 were required for CCF suppression (Fig.1A, Fig.S1F). These domains are involved in protein-protein interactions and are known to bind p53, especially p53 phosphorylated on serine 15(pSer15-p53)[28,29], suggesting a role for p53 in control of CCF formation. Confirming this interaction in senescent cells, pSer15-p53 coimmunoprecipitated with 53BP1 and vice versa (Fig.S1H,I). Consistent with the hypothesis that a 53BP1-p53 complex suppresses CCF formation, siRNA knockdown of p53, starting four days after senescence induction by irradiation, greatly increased CCF formation (Fig.1B). This timepoint was chosen because at this time the cells have exited the cell cycle but have not produced many CCF (Fig.1C). Conversely, activation of p53 after senescence induction by exogenous p53 expression, knockdown of MDM2, or by inhibition of MDM2 with two potent and selective clinical grade inhibitors, RG7388 and HDM201, suppressed CCF formation (Fig.1B-D; Fig.S1J-L)). Confirming an on-target effect of the MDM2 inhibitor, suppression of CCF formation by RG7388 was dependent on p53 (Fig.1B). siRNA-mediated knockdown of p53 and MDM2 was confirmed by western blot and immunofluorescence and revealed a strong negative correlation between p53 protein levels and CCF formation (Fig.S1M-P). MDM2i was titrated to the minimal dose required for SASP suppression as measured by expression of IL8 (Fig. S2A-D), and this dose was not senolytic and did not revert cell cycle arrest as measured by EdU incorporation assay (Fig.1E,F) Transcriptional profiling by bulk RNA-seq and qPCR of senescent cells treated with RG7388 or HDM201 showed a marked downregulation of inflammation-related gene ontologies associated with the SASP and expression of specific SASP genes, but did not affect expression of cell cycle-related genes (Fig.1G, Fig.S2E-H, Table S1). This suppression was most marked among NFkB target genes[30], and had a less marked effect on p53-[30], p21-[31], and p16-associated[31] secretomes (Fig.S2I, Table S1). These data are consistent with a senomorphic effect of p53 activation, specific to the NFkB-dependent inflammatory phenotype of senescent cells, but not senolysis nor a reversion of the entire senescence phenotype. Altogether, these data show that p53 is a potent and selective suppressor of CCF and the SASP, and that this function is pharmacologically targetable for specific senomorphic effect by MDM2i.

p53 activation promotes DNA repair

The mechanism of CCF formation is thought to depend primarily on DNA damage and autophagy[22,32,33]. In senescent cells treated with MDM2i, we consistently observed a decrease in CCF, as well as nuclear γH2A.X foci and total γH2A.X protein levels by western blot, suggesting that p53 activation may promote DNA repair in senescent cells (Fig.2A-C). p53 is known to regulate DNA double strand bread (DSB) repair through both local activity directly at sites of DNA damage and transcriptional activation of DNA repair factors [34,35]. Suggestive of p53 being a suppressor of CCF through a direct or local role in DNA repair[35], pSer15-p53 colocalized with intranuclear γH2A.X in senescent cells as previously reported[36], but was absent from CCF themselves (Fig.S3A), similar to the staining pattern of 53BP1 in senescent cells[32]. Also consistent with this model, suppression of CCF through activation of p53 with MDM2i or MDM2

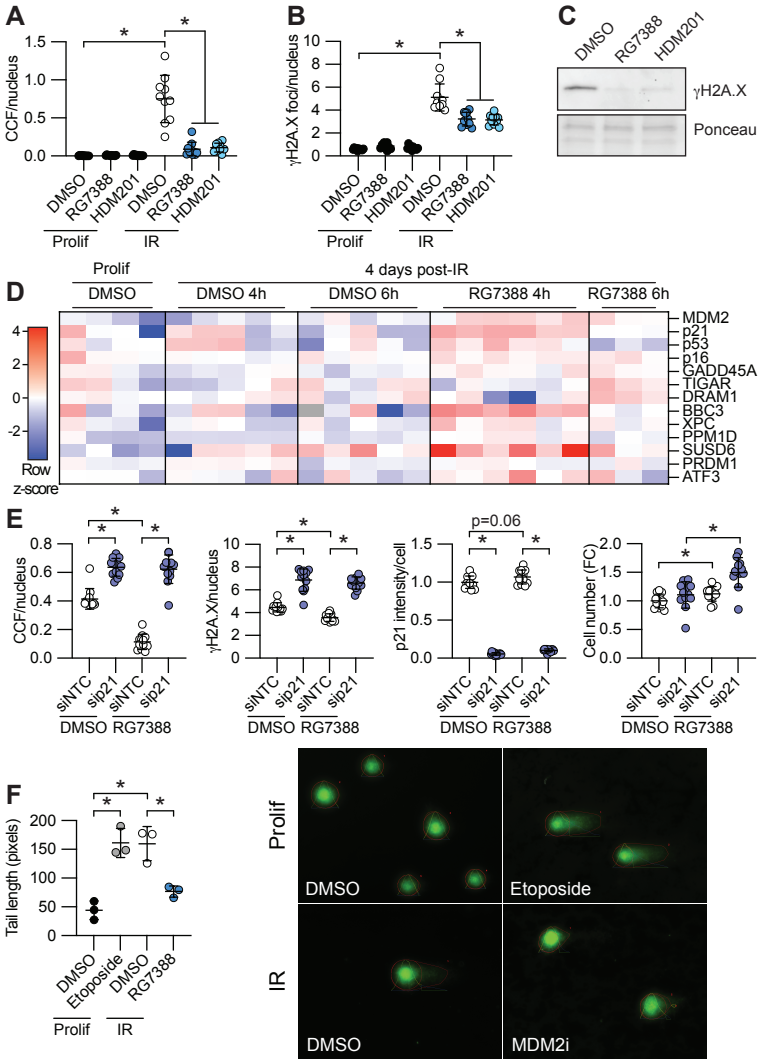

Figure 2: p53 activation promotes DNA repair. A) CCF formation and B) nuclear H2A.X foci number by IF in irradiation-induced IMR90 human fibroblasts. Each value represents one well of a culture plate, from a representative experiment. C) WB of H2A.X, n=2 observations. D) qPCR analysis of p53 target genes in cells 4 days after irradiation, treated for 4 or 6 hours with RG7388 or DMSO control, n=3-6, representative of 3 experiments. E) IF quantitation of CCF, nuclear H2A.X, p21, and cell number quantified by counting nuclei. F) Neutral comet assay and representative images. Each value represents one well of a culture plate, from a representative experiment. Data shown as means ±SEM, asterisk(*) indicates p<0.05 by Student's t-test. Prolif: proliferating control; NTC: non-targeting control; IR: ionizing radiation-induced senescence.

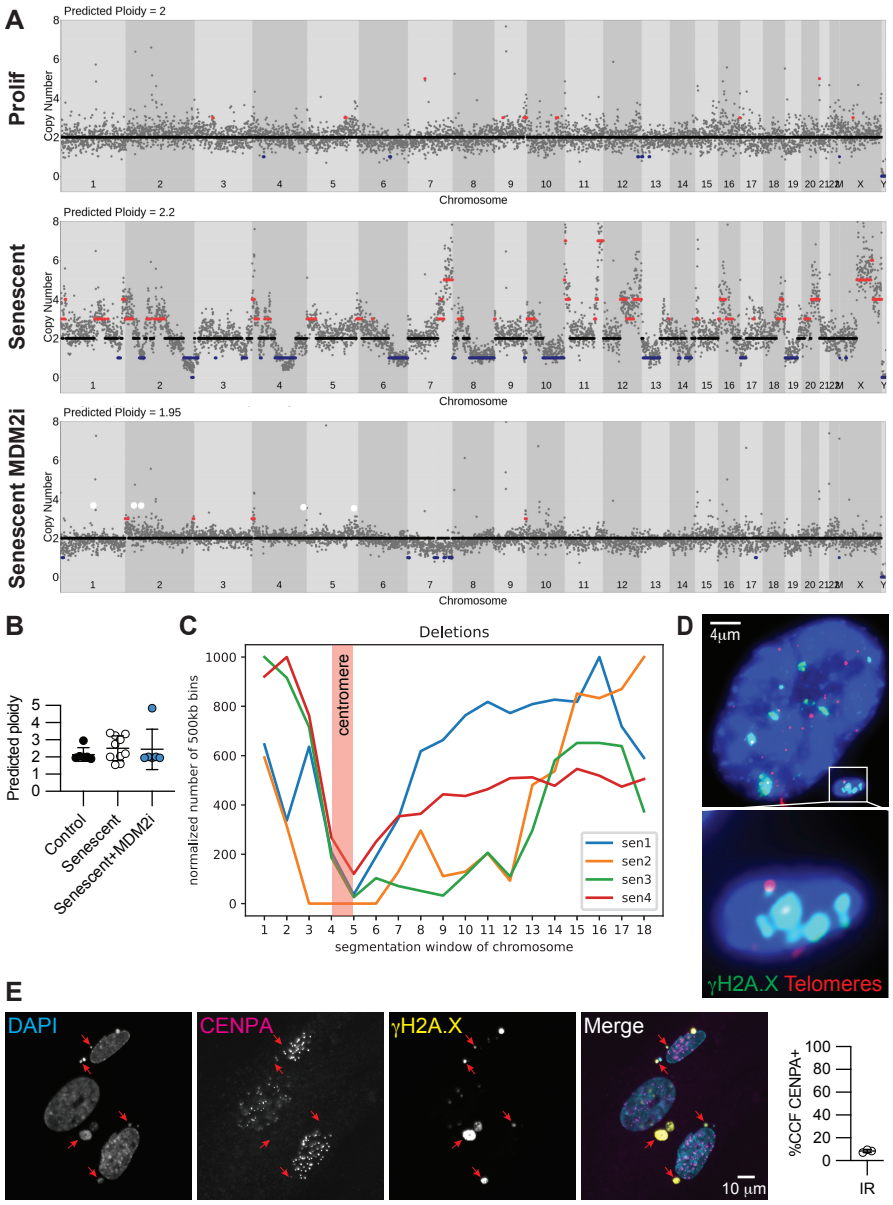

Figure 3: p53 preserves genome integrity in senescent cells. A) Representative single nucleus whole-genome plots showing copy number variations and B) predicted ploidy in irradiation-induced senescent IMR90 human fibroblasts, n=6, 10, 6 nuclei sequenced. C) Histogram of deletions, with each line an aggregation of all chromosomes per cell, n=4 senescent cells. Each chromosome is divided into 18 equal bins, where bins 1 and 18 are subtelomeric and bins 4-5 are pericentromeric. D) ImmunoFISH for telomeres and H2A.X, representative of n=3 independent experiments. E) IF for CENPA, with arrows marking CCF. For the quantitation, each marker represents approximately 3000 cells imaged for n=3 separate irradiations, representative of 2 independent experiments. Prolif: proliferating control.

knockdown increased colocalization of nuclear pSer15-p53 and γH2A.X foci at sites of intra-nuclear DNA damage in senescent cells, while p53 knockdown decreased colocalization (Fig.S3B-D). Most notably, across these treatments there was a direct correlation between intranuclear γH2A.X free of pSer15-pp53 and CCF, but an inverse correlation between pSer15-pp53 free of γH2A.X and CCF (Fig. S3D). However, the transcriptional role of p53 is also implicated in CCF suppression. Short-term treatment of senescent cells with RG7388 induced expression of p53 target genes, including several with known roles in DNA repair[37], such as CDKN1A, XPC, BBC3, and PPM1D (Fig.2D). CDKN1A (also known as p21) is thought to be required for efficient DNA repair, including repair of DSBs[38] and has been shown to suppress DDR-associated toxicity in senescent cells[39]. Knockdown of p21 in senescent cells using a shortened timeframe to avoid cell death in the absence of p21 increased γH2A.X foci and CCF formation, even in the presence of MDM2i, showing that p53-mediated activation of DNA repair and suppression of CCF formation is dependent on its transcriptional target p21 (Fig.2E). Confirming a role for p53 activation in DNA repair, treatment of senescent cells with RG7388 decreased DNA double strand break burden as measured by neutral comet assay (Fig.2F). We conclude that p53 activation promotes repair of DNA DSBs in senescent cells, a process that is very tightly linked to suppression of CCF.

p53 preserves genome integrity in senescent cells

We reasoned that p53's ability to promote DNA repair in senescent cells should underpin a role in preservation of genome integrity of senescent cells. To test this, we irradiated IMR90 cells and assessed genome copy number by single-nucleus genome resequencing after full establishment of senescence. Cells were treated with RG7388 five minutes after IR. In the absence of RG7388, single cell genome library preparation with a linear amplification-based approach (LIANTI)[40] showed large amplifications and deletions across the genomes of irradiated senescent cells with substantial heterogeneity, relative to normal proliferating cells that were diploid with few copy number variations (Fig.S4A). This was confirmed by a second PCR-based approach (Fig.3A, Fig.S4B). Remarkably, activation of p53 with RG7388 preserved genome integrity, as marked by diploid genome content with very few copy number variations in 5/6 cells sequenced (Fig.3A,B, Fig.S4B). Interestingly, we observed that these deletions tended to occur towards the telomeric ends of chromosomes, and only rarely included pericentromeric sequences (Fig.3C). Detection of telomeric and centromeric sequences in senescent cells by FISH confirmed that CCF contain telomeric DNA (Fig.3D). However, less than 10% of CCF contain the centromeric marker CENPA (Fig.3E). We conclude that p53 activation after acute genotoxic stress preserves genome integrity, presumably due to enhanced DNA repair, and this is tightly linked to suppression of telomeric DNA-containing CCF in senescent cells.

MDM2i is senomorphic in vivo

MDM2 inhibitors have been extensively developed as candidate cancer therapeutics and are generally considered highly specific *in vivo*[41,42]. To determine whether p53 activation can suppress SASP in vivo, we treated naturally aged mice with the clinical grade MDM2i, HDM201. Although HDM201 has been previously shown to have specific, on-target activity in mouse and rat tumor models[43,44], little is known about its activity in normal tissue, especially aged tissue. To test the effect of HDM201 on senescence phenotypes *in vivo*, we treated aged male and female mice for 14 days. This regimen was not associated with changes in whole blood counts, weight, or indices of liver pathology in either sex, suggesting that the treatment was well-tolerated (Fig.S5A-C). We focused our molecular analysis on liver, which is known to accumulate senescent cells and inflammation-associated pathologies with age[45]. Protein levels of p53 target

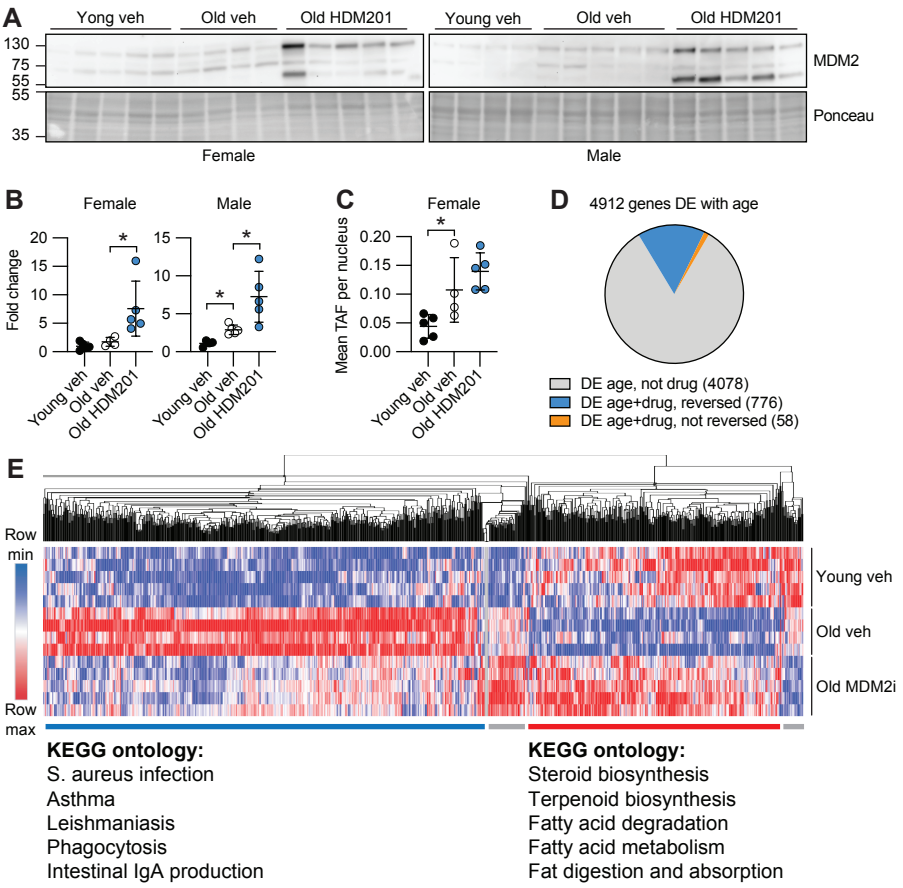

Figure 4: MDM2i is senomorphic in vivo. A) WB of the p53 target gene MDM2 in mouse liver and B) quantitation, n=4-5 per group. C) TAF assay in female mice, n=4-5 per group. D) Comparison of genes differentially expressed with age and HDM201 (drug) in liver by bulk RNA-seq, n=4-5 per group, and E) heatmap combining 776 “reversed” genes, where the change in expression of a gene is opposed by drug treatment, and 58 genes “not reversed”, with KEGG ontologies for major hierarchical clusters. F) Analysis of SenSig gene set in the same dataset, with KEGG ontologies for kmeans clusters of interest. Data shown as means ±SEM, asterisk(*) indicates $p<0.05$ by Mann-Whitney U test. Veh: vehicle control; DE: differentially expressed.

MDM2 measured by western blot were significantly increased in HDM201-treated mice compared to vehicle, confirming on-target engagement of the drug (Fig.4A,B). Interestingly, bulk RNA-seq of whole liver tissue showed extensive changes in gene expression in female mice treated with HDM201 compared to vehicle control, but few changes in gene expression were observed in male mice (Table S2), revealing a sex-dimorphic effect at this dose. In female mice, targeted analysis of established p53 target genes[46] showed a trend for increased expression of 45/103 genes (Fig.S5D), and statistically significant increased expression for 12 of these genes (Table S2). Assessment of liver senescent cell burden in female mice by telomere-associated DDR foci (TAF) staining showed an increase in TAF with age compared to young vehicle controls (5 month), but no change with HDM201 treatment compared to vehicle control (Fig.4C), consistent with the selective SASP-suppressive non-senolytic effect of MDM2i. Unbiased analysis showed 4912 genes differentially expressed in old vehicle-treated female mice compared to young vehicle female controls. Among these 4912 genes, 824 were differentially expressed with HDM201 treatment, of which the vast majority (776) showed reversal of the age-associated gene expression change (Fig.4D). Genes downregulated with age and upregulated with drug treatment were associated with sterol and fatty acid metabolic pathways, while genes upregulated with age and downregulated with drug treatment were associated with immune and inflammation pathways (Fig.4E, Table S2). These data show that p53 activation in aged female mice does not alter senescent cell burden, but reverses an age-associated transcriptional signature, supporting an anti-inflammatory, senomorphic activity of MDM2i *in vivo*.

Mitochondria suppress p53 activity in senescence

We have previously shown that mitochondrial stress drives CCF formation in senescent cells, and ablation of mitochondria by Parkin-mediated forced mitophagy[47] in senescent cells suppresses CCF formation[22] and SASP[22,48]. Thus, mitochondria and p53 are seemingly antagonistic regulators of CCF in senescence. Accordingly, we set out to test the relationship between them. To do this, we knocked down p53 in senescent IMR90 cells with or without ablation of mitochondria. Consistent with our previous work, ablation of mitochondria suppressed CCF formation and increased intranuclear γH2A.X foci number[22] (Fig.5A, Fig.S6A). However, although knockdown of p53 alone increased CCF formation and expression of SASP, cells with both ablation of mitochondria and knockdown of p53 had very few CCF and showed greatly increased and altered γH2A.X staining, with marked redistribution of γH2A.X staining throughout the nucleus, compared to cells with mitochondria treated with non-targeting siRNA (Fig.5B, Fig.S6A). This result shows that ablation of mitochondria is dominant to inactivation of p53 in terms of CCF formation and SASP but not intranuclear γH2A.X accumulation, suggesting that mitochondria are required for CCF formation and expression of the SASP at a step downstream of p53-mediated DNA repair.

Because CCF remove damaged DNA from the nucleus, a driver of p53 activation, we further reasoned that CCF and hence mitochondria might indirectly regulate p53 activity. Specifically, we hypothesized that forced mitophagy in senescent cells would activate p53 through activation of DNA damage signaling. Indeed, ablation of mitochondria in senescent cells greatly induced expression of p53 target genes in two different primary fibroblast strains (Fig.5C, Fig.S6B) and was accompanied by increased intranuclear γH2A.X and pS15-p53 (Fig.5B, Fig.S6A), consistent with the idea that p53 activation results from elevated DNA damage and the DNA damage response pathway. To test this directly, we inhibited the kinase ATM, which activates p53 in response to DNA damage by phosphorylation of serine 15[49,50]. Pharmacological inhibition of ATM blocked transcriptional activation of p21 in response to ablation of mitochondria, suggesting that mitochondria control of p53 activity is, at least in part, ATM-dependent (Fig.5D). These data show

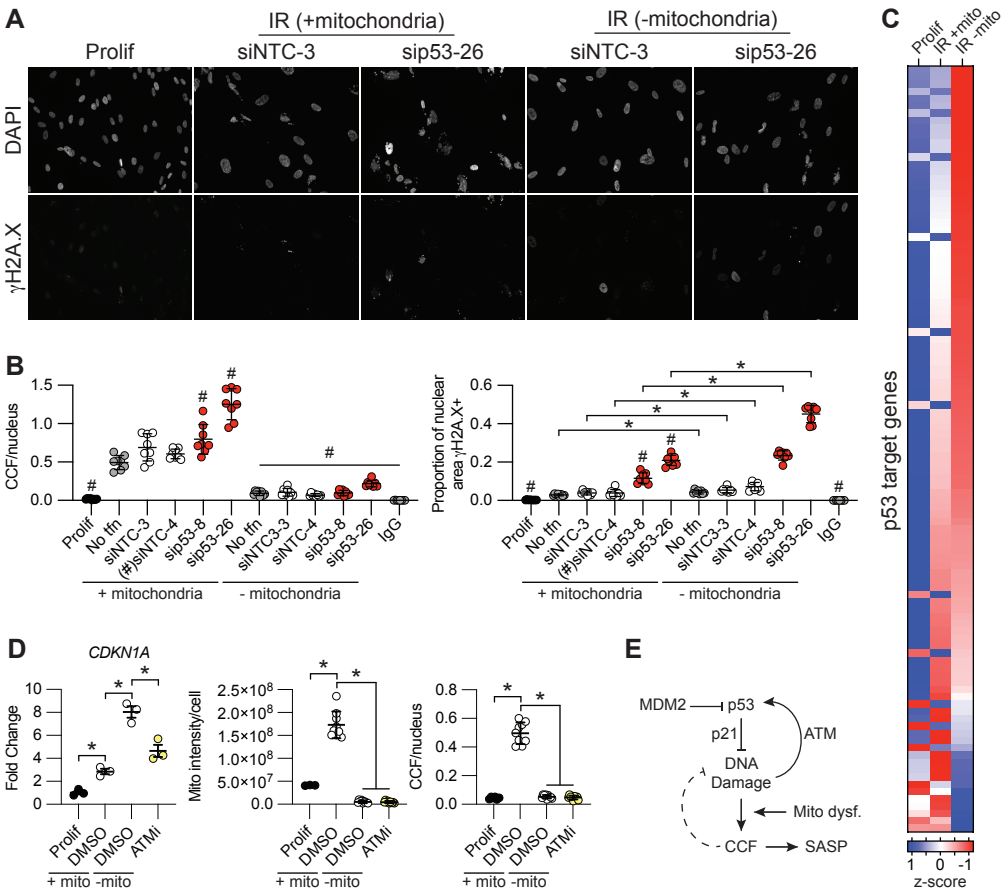

Figure 5: Mitochondria suppress p53 activity in senescence. A) IF representative images and B) quantitation of CCF and proportion of the nucleus staining positive for gH2AX in irradiation-induced senescent Parkin-overexpressing IMR90 human fibroblasts. Each value represents an individual well from a culture plate, from a representative experiment. Numbering indicates individual siRNA sequences. C) p53 target gene expression by RNAseq, average of n=3 per group shown. D) qPCR of CDKN1A and corresponding IF quantitation of mitochondria content and CCF. E) Model describing a mitochondria-regulated p53-CCF circuit. Data shown as means ±SEM, asterisk(*) indicates p<0.05 by t-test, (#) in panel B indicates p<0.05 vs siNTC-4. Prolif: proliferating control; NTC: non-targeting control; No tfn: no transfection control; IR: ionizing radiation-induced senescence.

that mitochondria in senescent cells suppress p53 activity, in part through an ATM-dependent feedback pathway.

Discussion

These data provide evidence for a mitochondria-regulated p53-CCF circuit in senescent cells (Fig.5E). This circuit controls DNA repair, genome integrity and SASP. p53 suppresses CCF formation and the SASP tightly linked to DNA repair, a pathway which is subject to feedback regulation by mitochondria. We show that activation of this pathway preserves genome integrity in senescent cells. The p53-CCF circuit is a potential target for anti-inflammatory and genome-stabilizing healthy aging interventions.

By single nucleus genome re-sequencing, we observed large deletions on the order of tens of millions of kilobases that tended to occur at the telomeric ends of chromosomes. CCF contained telomeres but not centromeres, suggesting that double-strand breaks are more likely to generate CCF if they are close to the end of a chromosome. Additional evidence from the literature shows that specific generation of DNA damage at telomeres is sufficient for CCF formation[51]. However, we cannot formally exclude an alternate model, that the mechanism of chromatin loss from the ends of chromosomes is instead dependent on preferential retention of centromeres, which are known to be distended in senescence[52]. p53 is known as the “guardian of the genome”, in part by suppressing genome instability in precancerous cells[35]. Although many mechanisms are implicated, recent work has shown that p53 loss in the course of cancer evolution leads to deterministic loss of genome integrity on an individual cell basis[53,54], perhaps consistent with our observation of a cell-intrinsic role for p53 in promoting genome stability in irradiation-induced senescence.

It has previously been reported that p53 suppresses the SASP [2,55], consistent with the observation that p53 activity declines in senescence after cell cycle exit, while SASP increases[56]—but the mechanism of SASP suppression by p53 has been unclear. We show that p53 suppresses formation of CCF, which are known to activate the SASP through a cGAS-STING pathway [23-26]. Additionally, this finding integrates our previous observations that dysfunctional mitochondria in senescent cells drive CCF formation and SASP [22,48]. Altogether, we propose a model in which p53 preserves genome integrity on a single-cell basis by promoting repair of DNA DSBs. In senescent cells, this pathway is suppressed by mitochondrial dysfunction, which instead drives resolution of DNA damage by cytosolic expulsion of the damaged DNA as CCF. This expulsion appears to indirectly downregulate p53 and to require a second mitochondria-driven pathway independent of p53, perhaps related to autophagy [33].

The role of p53 in aging is unclear—genetic manipulation of the p53 pathway is associated with either longevity or accelerated aging, depending on context[57]. The MDM2i UBX0101 has been explored as a senolytic in the context of osteoarthritis[58], although a phase 2 clinical trial failed to demonstrate efficacy in humans[59]. Recently, the MDM2i BI01 was shown to have senolytic activity in aged mouse muscle[60]. We show the MDM2i HDM201 is potentially senomorphic in mouse liver. However, in our in vitro models, we observe only SASP-suppressive senomorphic activity, not senolytic activity. We show the MDM2i HDM201 is potentially senomorphic in mouse liver. The suppression of inflammation-associated gene expression signature we observe via this p53-CCF circuit is consistent with a growing literature on the anti-inflammatory effects of MDM2i in vivo[61]. A better understanding of MDM2 inhibitors in experimental aging models could be a useful tool in the pursuit of interventions to promote healthy aging in humans.

305 **Methods**
306
307 *Animals:* This study was approved by the Institutional Animal Care and Use Committee at Sanford
308 Burnham Prebys MDI. C57BL6 mice were purchased from Jackson Labs and Charles River and
309 group housed under specific pathogen free conditions with ad libitum access to water and food
310 (Teklad 2018). Mice were treated with 10 mg/kg HDM201 (Novartis) suspended in phosphate-
311 buffered methylcellulose according to the manufacturer's instructions (0.5% methylcellulose in
312 phosphate buffer, pH6.8, 50mM) by daily oral gavage in the morning. Mice were monitored daily
313 and weighed every 2-3 days during treatment. After 14 days of treatment, mice were euthanized
314 by CO2 asphyxiation in the morning, and tissues were fixed in 10% neutral buffered formalin
315 (Epredia 9400-1) or flash frozen in liquid nitrogen, either whole or in OCT (Tissue-Tek 4583).
316 Whole blood was counted using a hematology analyzer (Abaxis VetScan HM5).
317
318 *Cell culture, senescence induction, and drug treatments:* IMR90 primary human fibroblasts were
319 grown at 37°C, 3.5% O2, 5% CO2, in Dulbecco's modified Eagle's medium (Gibco 10313-121)
320 with 10% FBS (Corning 35-0-11-CV), 1% penicillin/streptomycin (Gibco 15140-122) and 2 mM
321 glutamine (Gibco 25030-081). Cells were checked routinely for mycoplasma contamination. IR
322 senescence was induced by 20 Gray x-ray irradiation of 20-30% confluent cells. Cells were split
323 after returning to confluence in 3 days, then treated with MDM2 inhibitors, RG7388 (Selleckchem)
324 and HDM201 (Novartis), starting day 4 after irradiation or day 5 after irradiation in experiments
325 that also included siRNA treatment, unless otherwise noted. For longer-term treatments, drugs
326 were replaced by media change every 3 days. IMR90 cells exogenously expressing Parkin and
327 the method for mitochondria ablation are previously described (Vizioli). 293T cells were
328 purchased from ATCC.
329
330 *Plasmids:* pLV-hPGK-HA-53BP1-puro and pLV-EF1A-FLAG-p53-puro constructs were
331 generated by Vectorbuilder. Mutations to 53BP1 are described in Fig. S1.
332
333 *Lentivirus infection:* For 53BP1 exogenous expression, lentivirus was generated from 293T cells
334 transfected with expression vector, VSVG envelope vector, and pMD2.G packaging vector in
335 lipofectamine 2000 (Invitrogen 52887). Virus was collected over 3 days, then concentrated by
336 ultracentrifugation. For p53 exogenous expression, concentrated lentivirus was generated by the
337 SBP viral vector core facility using a proprietary protocol. Concentrated virus was titrated to the
338 minimum amount required for >90% cell viability after puromycin selection (8 ug/mL for 72 hours).
339 Infections were overnight (16 hours), in the presence of 8 ug/mL polybrene (Millipore TR-1003-
340 G).
341
342 *siRNA transfection*: Senescent cells were transfected 4 days after irradiation with 100 nM siRNA
343 (Dharmacon siGENOME) in 0.8% Dharmafect reagent (Dharmacon) according to manufacturer's
344 recommendations. Experiments used a pool of four siRNAs per gene unless otherwise noted.
345 Cells were changed into regular media 18-20 hours later, except sip21 experiments.
346
347 *Antibodies*: The following primary antibodies were used: 53BP1 (Cell Signaling Technology
348 Cat#4937, RRID:AB_10694558), ATM (D2E2) (Cell Signaling Technology Cat#2873,
349 RRID:AB_2062659), CENPA (Thermo Fisher Scientific Cat#MA1-20832, RRID:AB_2078763),
350 Cyclin A (Santa Cruz Biotechnology Cat#sc-271682, RRID:AB_10709300), ANTI-FLAG M2
351 (Sigma-Aldrich Cat#F3165-2MG, RRID:AB_259529), Phospho-Histone H2A.X (Ser139)
352 (Millipore Cat#05-636, RRID:AB_309864, Active Motif Cat#39117, RRID:AB_2793161), HA-
353 probe (F-7) (Santa Cruz Biotechnology Cat#sc-7392, RRID:AB_627809), IgG control (Vector
354 Laboratories Cat#I-1000, RRID:AB_2336355, Vector Laboratories Cat#I-2000,
355 RRID:AB_2336354), IL8 (Abcam Cat#ab18672, RRID:AB_444617), MDM2 (Cell Signaling

356 Technology Cat#51541, RRID:AB_2936381), p21 (Santa Cruz Biotechnology Cat#sc-817,
357 RRID:AB_628072), p53 (Santa Cruz Biotechnology Cat#sc-126, RRID:AB_628082, Leica
358 Biosystems Cat#NCL-p53-CM5p, RRID:AB_563933), Phospho-p53 (Ser15) (Cell Signaling
359 Technology Cat#9284S, RRID:AB_331464), Phospho-ATM (Ser1981) (Abcam Cat#ab81292,
360 RRID:AB_1640207), TOMM20 (Abcam Cat#ab56783, RRID:AB_945896). The following
361 secondary antibodies were used: Goat anti-Mouse IgG, IgM (H+L) HRP (Thermo Fisher Scientific
362 Cat#31446, RRID:AB_228318), Goat anti-Rabbit IgG, (H+L) HRP (Millipore Cat#AP307P,
363 RRID:AB_92641), Goat anti-Mouse IgG (H+L), Alexa Fluor™ 594 (Thermo Fisher Scientific
364 Cat#A11032, RRID:AB_2534091), Goat anti-Rabbit IgG (H+L), Alexa Fluor™ 488 (Thermo Fisher
365 Scientific Cat#A11008, RRID:AB_143165).
366
367 *Western blot:* For cells, blotting was done as previously described[62]. Briefly, cells were lysed in
368 modified RIPA buffer (50 mM Tris-Cl pH 7.5, 0.25% sodium deoxycholate, 150 mM NaCl, 10 mM
369 EDTA, 0.1% SDS, 1% Igepal, 1x dual protease and phosphatase inhibitor (Thermo 1861281))
370 and lysates were cleared by >20000g centrifugation. Protein was quantified by BCA assay (Pierce
371 23225), mixed with sample buffer, run on precast gels (Biorad), and transferred either with a Turbo
372 semidry system (Biorad), or for 53BP1 experiments wet transfer in tris-glycine buffer (Biorad) with
373 5% methanol. Membranes were blocked in milk and imaged by ECL (Thermo 34095, Biorad
374 Chemidoc). For mouse liver tissue, samples were lysed in modified RIPA buffer using a Bertin
375 Technologies Precellys tissue disruptor.
376
377 *Immunoprecipitation:* Protein G Dynabead-antibody complexes were prepared as previously
378 described[22]. Cells were washed 4 times in PBS, scraped in EBC500 (50 mM Tris-Cl pH 8, 500
379 mM NaCl, 0.5% Igepal, 2.5 mM MgCl2) with benzonase (250 U/mL), and lysed by rotating 30
380 minutes at 4°C. Protein was quantified by BCA assay. Immunoprecipitations were run overnight
381 at 4°C, washed 7 times in NETN (20 mM Tris-Cl pH 8, 100 mM NaCl, 1 mM EDTA, 0.5% Igepal),
382 and eluted in sample buffer.
383
384 *Immunofluorescence:* Cells were plated on PhenoPlate™ 96-well microplates (PerkinElmer),
385 stained as described previously[22], and imaged on a Nikon T2 microscope with automated image
386 capture. Images were analyzed in NIS Elements using rolling ball background subtraction,
387 thresholding, size exclusion, and automated partitioning to identify features.
388
389 *TAF staining and Immuno FISH*: Staining was done as previously described[21].
390
391 *Comet assay:* This assay was carried out following manufacturer's instruction for the neutral
392 comet SCGE assay (Enzo, #ADI-900-166). Slides were placed flat in the dark at 4C in the dark
393 for 30 minutes. Slides were immersed in pre-chilled lysis solution (2.5M NaCl, 100mM EDTA
394 pH10, 10mM Tris Base, 1% sodium lauryl sarcosinate, 1% Triton x-100, Catalog No.4250-050-
395 01) for 45 minutes. Electrophoresis was performed in TAE buffer (40mM Tris base, 20mM acetic
396 acid, 1mM EDTA disodium salt dihydrate) at 30V for 15 minutes at room temperature. Automated
397 comet analysis was performed using an open-source tool in ImageJ (Gyori et al 2014).
398
399 *qPCR:* Cells were lysed in Trizol (Ambion 15596026) and RNA was isolated using either a
400 commercial kit (53BP1 and MDM2i RNAseq experiments; Direct-zol RNA Miniprep Kits, Zymo
401 Research Cat#R2050) or with chloroform according to the manufacturer's protocol. RNA was
402 converted to cDNA (RevertAid Reverse Transcriptase, Thermo Fisher Scientific Cat#EP0441,
403 Ribolock RNase Inhibitor, Thermo Fisher Scientific Cat#EO0381, 5x reaction buffer for RT,
404 Thermo Fisher) and gene expression quantified by a standard SYBR-based approach
405 (PowerUp™ SYBR™ Green Master Mix for qPCR, Applied Biosystems Cat#A25741,
406 QuanStudio™ 6 Felx Real-Time PCR System, 384-well, Applied Biosystems Cat#4485691).

RNA-seq: RNA was quantified by bioanalyzer and library preps were made by the SBP genomics core. Sequencing was done by the SBP genomics core or at UCSD Institute for Genomic Medicine. For analysis, raw fastq files were aligned to hg19 (53BP1 OE RNAseq) or hg38 (MDM2i in cell culture RNAseq), or mm10 (MDM2i in mice RNAseq) using STAR[63] 2-pass pipeline. Reads were filtered, sorted and indexed by SAMtools[64]. FPKM were generated using CuffLinks[65] for downstream visualization. Genome tracks (bigWig files) were obtained by Deeptools[66]. Raw read counts were obtained by HTSeq[67] for differential analysis. Differentially expressed genes were obtained by DESeq2[68]. KEGG gene ontology was run using WebGestalt[69], gene lists were compared using Venny2.1(https://bioinfogp.cnb.csic.es/tools/venny/index.html), and heatmaps were generated using Morpheus (https://software.broadinstitute.org/Morpheus).

Single cell genome resequencing: Cells were trypsinized, washed in PBS, and resuspended at 20x cell pellet volume in cold nuclear isolation buffer A with digitonin (50 nM HEPES pH 7.3, 150 mM NaCl, 1x dual protease and phosphatase inhibitor, 25 μg/mL digitonin) by pipetting. The suspensions were rotated at 4°C for 30 minutes, then centrifuged at 500g for 5 minutes at 4°C. Nuclear pellets were washed twice with cold NIB-250 buffer (250 mM sucrose, 15mM Tris-Cl pH 7.5, 60 mM KCl, 15 mM NaCl, 5 mM MgCl2, 1 mM CaCl2) and resuspended in sorting buffer (DPBS with 2% FBS, 0.5 mM spermidine, 500 ng/mL DAPI). Nuclei were sorted by FACSAriaII with a 100um nozzle (see also Fig.S7) into individual strip tubes, and libraries were generated by LIANTI[40] or PicoPLEX Gold (Takara Bio). Libraries were sequenced by NOVAseq (Illumina) and analyzed in Ginkgo. For analysis, the first 14 bases of both R1 and R2 reads were trimmed using CutAdapt[70]. Trimmed reads were then aligned to hg38 using Bowtie2[71]. sam files were transferred to bam files then sorted and index using SAMtools[64]. Duplicates were removed using picard tools (https://broadinstitute.github.io/picard/) MarkDuplicates function. Copy number variation profiles were obtained via Ginkgo[72].

Histology: Formalin-fixed liver tissue was paraffin embedded, sectioned, and H&E stained by the SBP histology core using standard approaches. Images were scored by a trained pathologist (C.M.) for age-associated liver pathology.

Statistical analysis: Statistical significance for routine assays was calculated in Graphpad Prism, using $p<0.05$ as a threshold. For cell culture experiments, pairwise comparisons were done using Student's t-test assuming unequal variance between groups. Simple linear regressions were calculated in Graphpad Prism. For animal experiments, pairwise comparisons were done using a Mann-Whitney U test. Data are representative of at least three independent experiments, unless otherwise indicated.

Acknowledgements

We would like to thank Dr. Sha Li, Andrew Davis, and Adriana Charbono for technical support with mouse experiments. This work was supported by K99 AG073450 and F32 AG066459 (to KNM); the Glenn Foundation for Medical Research Postdoctoral Fellowship PD19131 and the AFAR Reboot Fund (to ND); P30CA03199 (YA); R01AG082785 (to ZD); the Intramural Research Program of the National Institutes of Health, National Cancer Institute (1ZIABC011884) (to JL and CC); R01AG68048, UG3CA268103 and R01AG82708 (to JFP) and P01 AG031862 and R01 AG071861 (to PDA).

Author contributions

Conceptualization: KNM, BL, HRPH, SP, CCM, TL, ND, ZD, PDA. Methodology: ND, ABL, JL, YA, RP, GG, CC. Data generation and analysis: KNM, BL, HRPH, XL, APH, SP, CCM, SGV, SW, ABL, YA, CM. Writing: KNM, BL, ZD, PDA. Funding: KNM, PDA. Supervision: CC, JFP, PDA.

Competing interests

The authors have no competing interests.

Materials & Correspondence

Correspondence and requests for materials should be addressed to KNM and PDA.

Figure legends

Figure 1: p53 suppresses CCF formation. A) CCF staining by IF in irradiation-induced senescent IMR90 human fibroblasts. Each value represents an individual well from a culture plate, from a representative experiment. B) Western blot and CCF staining by immunofluorescence using timeframe described in Fig.S1J, representative of n=2 experiments. C) CCF staining by IF, average of 3 experiments. D) CCF and FLAG staining by IF. Each value represents a separate infection in a single experiment, representative of n=3 experiments. E) Cell number normalized to DMSO control for each group. F) EdU incorporation assay. G) Differentially expressed genes by RNAseq, n=3 per group with summarized KEGG ontology for each major cluster. See Table S1 for detailed ontology. Data shown as means ±SEM, asterisk(*) indicates $p<0.05$ by Student's t-test. Prolif: proliferating control; EV: empty vector; NTC: non-targeting contro; IR: ionizing radiation-induced senescence.

Figure 2: p53 activation promotes DNA repair. A) CCF formation and B) nuclear γH2A.X foci number by IF in irradiation-induced IMR90 human fibroblasts. Each value represents one well of a culture plate, from a representative experiment. C) WB of γH2A.X, n=2 observations. D) qPCR analysis of p53 target genes in cells 4 days after irradiation, treated for 4 or 6 hours with RG7388 or DMSO control, n=3-6, representative of 3 experiments. E) IF quantitation of CCF, nuclear γH2A.X, p21, and cell number quantified by counting nuclei. F) Neutral comet assay and representative images. Each value represents one well of a culture plate, from a representative experiment. Data shown as means ±SEM, asterisk(*) indicates $p<0.05$ by Student's t-test. Prolif: proliferating control; NTC: non-targeting control; IR: ionizing radiation-induced senescence.

Figure 3: p53 preserves genome integrity in senescent cells. A) Representative single nucleus whole-genome plots showing copy number variations and B) predicted ploidy in irradiation-induced senescent IMR90 human fibroblasts, n=6, 10, 6 nuclei sequenced. C) Histogram of deletions, with each line an aggregation of all chromosomes per cell, n=4 senescent cells. Each chromosome is divided into 18 equal bins, where bins 1 and 18 are subtelomeric and bins 4-5 are pericentromeric. D) ImmunoFISH for telomeres and γH2A.X, representative of n=3 independent experiments. E) IF for CENPA, with arrows marking CCF. For the quantitation, each marker represents approximately 3000 cells imaged for n=3 separate irradiations, representative of 2 independent experiments. Prolif: proliferating control.

Figure 4: MDM2i is senomorphic in vivo. A) WB of the p53 target gene MDM2 in mouse liver and B) quantitation, n=4-5 per group. C) TAF assay in female mice, n=4-5 per group. D) Comparison of genes differentially expressed with age and HDM201 (drug) in liver by bulk RNA-seq, n=4-5 per group, and E) heatmap combining 776 "reversed" genes, where the change in expression of a gene is opposed by drug treatment, and 58 genes "not reversed", with KEGG ontologies for major hierarchical clusters. F) Analysis of SenSig gene set in the same dataset, with KEGG ontologies for kmeans clusters of interest. Data shown as means ±SEM, asterisk(*) indicates $p<0.05$ by Mann-Whitney U test. Veh: vehicle control; DE: differentially expressed.

Figure 5: Mitochondria suppress p53 activity in senescence. A) IF representative images and B) quantitation of CCF and proportion of the nucleus staining positive for gH2AX in irradiation-induced senescent Parkin-overexpressing IMR90 human fibroblasts. Each value represents an individual well from a culture plate, from a representative experiment. Numbering indicates individual siRNA sequences. C) p53 target gene expression by RNAseq, average of n=3 per group shown. D) qPCR of CDKN1A and corresponding IF quantitation of mitochondria content and CCF. E) Model describing a mitochondria-regulated p53-CCF circuit. Data shown as means ±SEM, asterisk(*) indicates $p<0.05$ by t-test, (#) in panel B indicates $p<0.05$ vs siNTC-4. Prolif: proliferating control; NTC: non-targeting control; No tfn: no transfection control; IR: ionizing radiation-induced senescence.

Figure S1: Related to Figure 1. A) Irradiation-induced senescent IMR90 human fibroblasts ectopically expressing 53BP1 or empty vector, IL8 WB, B) qPCR validation, and C) RNA-seq PCA. D) Hierarchical clustering of differentially expressed genes and E) KEGG ontology of cluster indicated by dashed box. F) 53BP1 protein map with major domains targeted by mutagenesis, and ability of these mutants to suppress CCF formation by IF. G) Expression of 53BP1 mutants by WB. H) IP of pS15-p53 or 53BP1, n=1 experiment. I) IP of pS15-p53 and ponceau stain, n=1 experiment. J) Schematic of siRNA experiments. K) nuclear gH2AX and L) cell number related to Fig.1D. M-P) Deconvolution of siRNA pools, assessing CCF, p53, and nuclear gH2AX by IF, n=1 experiment. Data shown as means ±SEM, asterisk(*) indicates $p<0.05$ by Student's t-test. Prolif: proliferating control; IR: ionizing radiation-induced senescence; wt: wild-type; EV: empty vector; OE: overexpression; en: endogenous transcript; ex: exogenous transcript; NTC: non-targeting control; IR: ionizing radiation-induced senescence.

Figure S2: Related to Figure 1. A-D) MDM2i dose-response curves in irradiation-induced senescent IMR90 human fibroblasts by IL8 WB, n=1 experiment each. E) qPCR validation and F) RNA-seq PCA for MDM2i treatment related to Fig.1G. G) Venn diagram of DE genes. H) Left to right: NFkB, p53, p21, and p16-associated secretomes. Data shown as means ±SEM, asterisk(*) indicates $p<0.05$ by Student's t-test. P: proliferating control; IR: ionizing irradiation-induced senescence.

Figure S3: Related to Figure 2. A) Representative IF image of gH2AX and pS15-p53 colocalization and B) IF quantitation of colocalization. C) Quantitation of "p53-free" gH2AX foci not colocalized with pS15-p53, from same dataset as Fig.1B, and D) correlations. Data shown as means ±SEM, asterisk(*) indicates $p<0.05$ by Student's t-test. Prolif: proliferating control; NTC: non-targeting control.

Figure S4: Related to Figure 3. Whole genome CNV plots for all cells sequenced by A) LIANTI or B) PicoPLEX Gold approaches.

Figure S5: Related to Figure 4. A) Body weight, B) whole blood measures, and C) liver histology from mouse experiment in Fig.4, n=4-5. D) p53 target gene expression in female mice. Data shown as means ±SEM, asterisk(*) indicates $p<0.05$ by Mann-Whitney U test. V: vehicle; H: HDM201; Y: young; O: old; F: female; M: male.

Figure S6: Related to Figure 5. A) WB validation of mitochondrial ablation and p53 knockdown. B) p53 target genes with mitochondrial ablation in MRC5 fibroblasts, from ref[48]. IR: ionizing radiation-induced senescence.

Figure S7: Flow cytometry gating. A) Proliferating, B) Senescent, C) Senescent + MDM2i. Red marks correspond to individual sorted nuclei in Fig.S4B.

Table S1: RNAseq analysis from cell culture experiments.

Table S2: RNAseq analysis from mouse experiments.

References

1 Hayflick, L. & Moorhead, P. S. The serial cultivation of human diploid cell strains. *Exp Cell Res* **25**, 585-621 (1961).

2 Coppe, J. P. *et al.* Senescence-associated secretory phenotypes reveal cell-nonautonomous functions of oncogenic RAS and the p53 tumor suppressor. *PLoS biology* **6**, 2853-2868, doi:08-PLBI-RA-2566 [pii] 10.1371/journal.pbio.0060301 (2008).

3 McHugh, D. & Gil, J. Senescence and aging: Causes, consequences, and therapeutic avenues. *J Cell Biol* **217**, 65-77, doi:10.1083/jcb.201708092 (2018).

4 Moiseeva, V. *et al.* Context-dependent roles of cellular senescence in normal, aged, and disease states. *FEBS J* **290**, 1161-1185, doi:10.1111/febs.16573 (2023).

5 Baker, D. J. *et al.* Naturally occurring p16(Ink4a)-positive cells shorten healthy lifespan. *Nature* **530**, 184-189, doi:10.1038/nature16932 (2016).

6 Baker, D. J. *et al.* Clearance of p16Ink4a-positive senescent cells delays ageing-associated disorders. *Nature* **479**, 232-236, doi:nature10600 [pii] 10.1038/nature10600 (2011).

7 Zhu, Y. *et al.* Identification of a Novel Senolytic Agent, Navitoclax, Targeting the Bcl-2 Family of Anti-Apoptotic Factors. *Aging cell*, doi:10.1111/acel.12445 (2015).

8 Xu, M. *et al.* Senolytics improve physical function and increase lifespan in old age. *Nat Med* **24**, 1246-1256, doi:10.1038/s41591-018-0092-9 (2018).

9 Zhang, L. *et al.* Cellular senescence: a key therapeutic target in aging and diseases. *J Clin Invest* **132**, doi:10.1172/JCI158450 (2022).

10 Laberge, R. M. *et al.* MTOR regulates the pro-tumorigenic senescence-associated secretory phenotype by promoting IL1A translation. *Nat Cell Biol* **17**, 1049-1061, doi:10.1038/ncb3195 (2015).

11 Laberge, R. M. *et al.* Glucocorticoids suppress selected components of the senescence-associated secretory phenotype. *Aging cell* **11**, 569-578, doi:10.1111/j.1474-9726.2012.00818.x (2012).

12 Birch, J. & Passos, J. F. Targeting the SASP to combat ageing: Mitochondria as possible intracellular allies? *Bioessays* **39**, doi:10.1002/bies.201600235 (2017).

13 Georgilis, A. *et al.* PTBP1-Mediated Alternative Splicing Regulates the Inflammatory Secretome and the Pro-tumorigenic Effects of Senescent Cells. *Cancer Cell* **34**, 85-102 e109, doi:10.1016/j.ccell.2018.06.007 (2018).

14 Niedernhofer, L. J. & Robbins, P. D. Senotherapeutics for healthy ageing. *Nat Rev Drug Discov* **17**, 377, doi:10.1038/nrd.2018.44 (2018).

15 Xu, M. *et al.* JAK inhibition alleviates the cellular senescence-associated secretory phenotype and frailty in old age. *Proceedings of the National Academy of Sciences of the United States of America* **112**, E6301-6310, doi:10.1073/pnas.1515386112 (2015).

16 Yoshimoto, S. *et al.* Obesity-induced gut microbial metabolite promotes liver cancer through senescence secretome. *Nature* **499**, 97-101, doi:10.1038/nature12347 (2013).

17 Kang, C. *et al.* The DNA damage response induces inflammation and senescence by inhibiting autophagy of GATA4. *Science* **349**, aaa5612, doi:10.1126/science.aaa5612 (2015).

18 Freund, A., Patil, C. K. & Campisi, J. p38MAPK is a novel DNA damage response-independent regulator of the senescence-associated secretory phenotype. *EMBO J* **30**, 1536-1548, doi:10.1038/emboj.2011.69 (2011).
19 Miller, K. N. *et al.* Cytoplasmic DNA: sources, sensing, and role in aging and disease. *Cell* **184**, 5506-5526, doi:10.1016/j.cell.2021.09.034 (2021).
20 De Cecco, M. *et al.* L1 drives IFN in senescent cells and promotes age-associated inflammation. *Nature* **566**, 73-78, doi:10.1038/s41586-018-0784-9 (2019).
21 Victorelli, S. *et al.* Apoptotic stress causes mtDNA release during senescence and drives the SASP. *Nature*, doi:10.1038/s41586-023-06621-4 (2023).
22 Vizioli, M. G. *et al.* Mitochondria-to-nucleus retrograde signaling drives formation of cytoplasmic chromatin and inflammation in senescence. *Genes Dev*, doi:10.1101/gad.331272.119 (2020).
23 Dou, Z. *et al.* Cytoplasmic chromatin triggers inflammation in senescence and cancer. *Nature* **550**, 402-406, doi:10.1038/nature24050 (2017).
24 Gluck, S. *et al.* Innate immune sensing of cytosolic chromatin fragments through cGAS promotes senescence. *Nat Cell Biol* **19**, 1061-1070, doi:10.1038/ncb3586 (2017).
25 Yang, H., Wang, H., Ren, J., Chen, Q. & Chen, Z. J. cGAS is essential for cellular senescence. *Proceedings of the National Academy of Sciences of the United States of America* **114**, E4612-E4620, doi:10.1073/pnas.1705499114 (2017).
26 Takahashi, A. *et al.* Downregulation of cytoplasmic DNases is implicated in cytoplasmic DNA accumulation and SASP in senescent cells. *Nat Commun* **9**, 1249, doi:10.1038/s41467-018-03555-8 (2018).
27 Miller, K. N., Dasgupta, N., Liu, T., Adams, P. D. & Vizioli, M. G. Cytoplasmic chromatin fragments-from mechanisms to therapeutic potential. *Elife* **10**, doi:10.7554/eLife.63728 (2021).
28 Derbyshire, D. J. *et al.* Crystal structure of human 53BP1 BRCT domains bound to p53 tumour suppressor. *EMBO J* **21**, 3863-3872, doi:10.1093/emboj/cdf383 (2002).
29 Cuella-Martin, R. *et al.* 53BP1 Integrates DNA Repair and p53-Dependent Cell Fate Decisions via Distinct Mechanisms. *Mol Cell* **64**, 51-64, doi:10.1016/j.molcel.2016.08.002 (2016).
30 Wang, B. *et al.* Pharmacological CDK4/6 inhibition reveals a p53-dependent senescent state with restricted toxicity. *EMBO J* **41**, e108946, doi:10.15252/embj.2021108946 (2022).
31 Sturmlechner, I. *et al.* p21 produces a bioactive secretome that places stressed cells under immunosurveillance. *Science* **374**, eabb3420, doi:10.1126/science.abb3420 (2021).
32 Ivanov, A. *et al.* Lysosome-mediated processing of chromatin in senescence. *J Cell Biol* **202**, 129-143, doi:10.1083/jcb.201212110 (2013).
33 Dou, Z. *et al.* Autophagy mediates degradation of nuclear lamina. *Nature* **527**, 105-109, doi:10.1038/nature15548 (2015).
34 Williams, A. B. & Schumacher, B. p53 in the DNA-Damage-Repair Process. *Cold Spring Harbor perspectives in medicine* **6**, doi:10.1101/cshperspect.a026070 (2016).
35 Wang, Y. H. *et al.* Rapid recruitment of p53 to DNA damage sites directs DNA repair choice and integrity. *Proceedings of the National Academy of Sciences of the United States of America* **119**, e2113233119, doi:10.1073/pnas.2113233119 (2022).
36 Rodier, F. *et al.* DNA-SCARS: distinct nuclear structures that sustain damage-induced senescence growth arrest and inflammatory cytokine secretion. *Journal of cell science* **124**, 68-81, doi:jcs.071340 [pii]
10.1242/jcs.071340 (2011).
37 Kastenhuber, E. R. & Lowe, S. W. Putting p53 in Context. *Cell* **170**, 1062-1078, doi:10.1016/j.cell.2017.08.028 (2017).

38 Ticli, G., Cazzalini, O., Stivala, L. A. & Prosperi, E. Revisiting the Function of p21(CDKN1A) in DNA Repair: The Influence of Protein Interactions and Stability. *Int J Mol Sci* **23**, doi:10.3390/ijms23137058 (2022).
39 Yosef, R. *et al.* p21 maintains senescent cell viability under persistent DNA damage response by restraining JNK and caspase signaling. *EMBO J* **36**, 2280-2295, doi:10.15252/embj.201695553 (2017).
40 Chen, C. *et al.* Single-cell whole-genome analyses by Linear Amplification via Transposon Insertion (LIANTI). *Science* **356**, 189-194, doi:10.1126/science.aak9787 (2017).
41 Zhu, H. *et al.* Targeting p53-MDM2 interaction by small-molecule inhibitors: learning from MDM2 inhibitors in clinical trials. *J Hematol Oncol* **15**, 91, doi:10.1186/s13045-022-01314-3 (2022).
42 Stein, E. M. *et al.* Results from a First-in-Human Phase I Study of Siremadlin (HDM201) in Patients with Advanced Wild-Type TP53 Solid Tumors and Acute Leukemia. *Clin Cancer Res* **28**, 870-881, doi:10.1158/1078-0432.CCR-21-1295 (2022).
43 Chapeau, E. A. *et al.* Resistance mechanisms to TP53-MDM2 inhibition identified by in vivo piggyBac transposon mutagenesis screen in an Arf(-/-) mouse model. *Proceedings of the National Academy of Sciences of the United States of America* **114**, 3151-3156, doi:10.1073/pnas.1620262114 (2017).
44 Jeay, S. *et al.* Dose and Schedule Determine Distinct Molecular Mechanisms Underlying the Efficacy of the p53-MDM2 Inhibitor HDM201. *Cancer Res* **78**, 6257-6267, doi:10.1158/0008-5472.CAN-18-0338 (2018).
45 Ogrodnik, M. *et al.* Cellular senescence drives age-dependent hepatic steatosis. *Nat Commun* **8**, 15691, doi:10.1038/ncomms15691 (2017).
46 Fischer, M. Census and evaluation of p53 target genes. *Oncogene* **36**, 3943-3956, doi:10.1038/onc.2016.502 (2017).
47 Tait, S. W. *et al.* Widespread mitochondrial depletion via mitophagy does not compromise necroptosis. *Cell reports* **5**, 878-885, doi:10.1016/j.celrep.2013.10.034 (2013).
48 Correia-Melo, C. *et al.* Mitochondria are required for pro-ageing features of the senescent phenotype. *EMBO J*, doi:10.15252/embj.201592862 (2016).
49 Banin, S. *et al.* Enhanced phosphorylation of p53 by ATM in response to DNA damage. *Science* **281**, 1674-1677. (1998).
50 Canman, C. E. *et al.* Activation of the ATM kinase by ionizing radiation and phosphorylation of p53. *Science* **281**, 1677-1679. (1998).
51 Barnes, R. P. *et al.* Telomeric 8-oxo-guanine drives rapid premature senescence in the absence of telomere shortening. *Nat Struct Mol Biol* **29**, 639-652, doi:10.1038/s41594-022-00790-y (2022).
52 Cruickshanks, H. A. *et al.* Senescent cells harbour features of the cancer epigenome. *Nat Cell Biol* **15**, 1495-1506, doi:10.1038/ncb2879 (2013).
53 Baslan, T. *et al.* Ordered and deterministic cancer genome evolution after p53 loss. *Nature* **608**, 795-802, doi:10.1038/s41586-022-05082-5 (2022).
54 Funnell, T. *et al.* Single-cell genomic variation induced by mutational processes in cancer. *Nature* **612**, 106-115, doi:10.1038/s41586-022-05249-0 (2022).
55 Wiley, C. D. *et al.* Small-molecule MDM2 antagonists attenuate the senescence-associated secretory phenotype. *Scientific reports* **8**, 2410, doi:10.1038/s41598-018-20000-4 (2018).
56 Sturmlechner, I. *et al.* Senescent cells limit p53 activity via multiple mechanisms to remain viable. *Nat Commun* **13**, 3722, doi:10.1038/s41467-022-31239-x (2022).
57 Wu, D. & Prives, C. Relevance of the p53-MDM2 axis to aging. *Cell Death Differ* **25**, 169-179, doi:10.1038/cdd.2017.187 (2018).

58 Jeon, O. H. *et al.* Local clearance of senescent cells attenuates the development of post-traumatic osteoarthritis and creates a pro-regenerative environment. *Nat Med* **23**, 775-781, doi:10.1038/nm.4324 (2017).
59 Lane, N. *et al.* A Phase 2, Randomized, Double-Blind, Placebo-Controlled Study of Senolytic Molecule Ubx0101 in the Treatment of Painful Knee Osteoarthritis. *Osteoarthr Cartilage* **29**, S52-S53 (2021).
60 Nolt, G. L. *et al.* Inhibition of p53-MDM2 binding reduces senescent cell abundance and improves the adaptive responses of skeletal muscle from aged mice. *Geroscience*, doi:10.1007/s11357-023-00976-2 (2023).
61 Wang, W. *et al.* Targeting MDM2 for novel molecular therapy: Beyond oncology. *Med Res Rev* **40**, 856-880, doi:10.1002/med.21637 (2020).
62 Miller, K. N. *et al.* PGC-1a integrates a metabolism and growth network linked to caloric restriction. *Aging cell* **18**, e12999, doi:10.1111/acel.12999 (2019).
63 Dobin, A. *et al.* STAR: ultrafast universal RNA-seq aligner. *Bioinformatics (Oxford, England)* **29**, 15-21, doi:10.1093/bioinformatics/bts635 (2013).
64 Danecek, P. *et al.* Twelve years of SAMtools and BCFtools. *Gigascience* **10**, doi:10.1093/gigascience/giab008 (2021).
65 Trapnell, C. *et al.* Transcript assembly and quantification by RNA-Seq reveals unannotated transcripts and isoform switching during cell differentiation. *Nat Biotechnol* **28**, 511-515, doi:10.1038/nbt.1621 (2010).
66 Ramirez, F. *et al.* deepTools2: a next generation web server for deep-sequencing data analysis. *Nucleic acids research* **44**, W160-165, doi:10.1093/nar/gkw257 (2016).
67 Putri, G. H., Anders, S., Pyl, P. T., Pimanda, J. E. & Zanini, F. Analysing high-throughput sequencing data in Python with HTSeq 2.0. *Bioinformatics (Oxford, England)* **38**, 2943-2945, doi:10.1093/bioinformatics/btac166 (2022).
68 Love, M. I., Huber, W. & Anders, S. Moderated estimation of fold change and dispersion for RNA-seq data with DESeq2. *Genome Biol* **15**, 550, doi:10.1186/s13059-014-0550-8 (2014).
69 Zhang, B., Kirov, S. & Snoddy, J. WebGestalt: an integrated system for exploring gene sets in various biological contexts. *Nucleic acids research* **33**, W741-748, doi:10.1093/nar/gki475 (2005).
70 Martin, M. Cutadapt removes adapter sequences from high-throughput sequencing reads. *EMBnet.journal* **17**, 10-12, doi:https://doi.org/10.14806/ej.17.1.200 (2011).
71 Langmead, B. & Salzberg, S. L. Fast gapped-read alignment with Bowtie 2. *Nat Methods* **9**, 357-359, doi:10.1038/nmeth.1923 (2012).
72 Garvin, T. *et al.* Interactive analysis and assessment of single-cell copy-number variations. *Nat Methods* **12**, 1058-1060, doi:10.1038/nmeth.3578 (2015).